

1 Current Biology. Report.

2 **Title: Hexadirectional modulation of high-frequency electrophysiological activity**
3 **in the human anterior medial temporal lobe maps visual space**

4 Authors: Tobias Staudigl,^{1,2,9,*} Marcin Leszczynski,^{3,4} Joshua Jacobs,⁵ Sameer A. Sheth,³ Charles E.

5 Schroeder,^{3,4} Ole Jensen,⁶ and Christian F. Doeller^{1,7,8**}

6

7 **Highlights**

- 8 • Hexadirectional modulation of human high-frequency electrophysiological activity
9 • Grid-like mapping of visual space in the human entorhinal cortex
10 • Grid-coding beyond environmental mapping during locomotion

11

12 **In Brief**

13 Staudigl et al. show grid-like modulation of human high-frequency activity in noninvasive
14 magnetoencephalographic and intracranial EEG recordings. The results indicate that the human
15 entorhinal cortex codes visual space in a grid-like manner, supporting the view that grid coding generalizes
16 beyond environmental mapping during locomotion.

17

18 ¹Donders Institute for Brain, Cognition, and Behaviour, Radboud University, Nijmegen, the Netherlands

19 ²Department of Neurosurgery, Cedars-Sinai Medical Center, Los Angeles, CA, USA

20 ³Cognitive Science and Neuromodulation Program, Department of Neurological Surgery, Columbia
21 University College of Physicians and Surgeons, New York, NY, USA

22 ⁴Translational Neuroscience Division, Nathan Kline Institute, Orangeburg, NY, USA

23 ⁵Department of Biomedical Engineering, Columbia University, New York, NY, USA

24 ⁶Centre for Human Brain Health, School of Psychology, University of Birmingham, Birmingham, UK

25 ⁷Kavli Institute for Systems Neuroscience, Centre for Neural Computation, Egil and Pauline Braathen and
26 Fred Kavli Centre for Cortical Microcircuits, NTNU and St. Olavs Hospital, Trondheim, Norway

27 ⁸Max Planck Institute for Human Cognitive and Brain Sciences, Leipzig, Germany

28 ⁹Lead Contact

29 *Correspondence: tobias.staudigl@cshs.org

30 **Correspondence: christian.doeller@ntnu.no

31

32 **Summary**

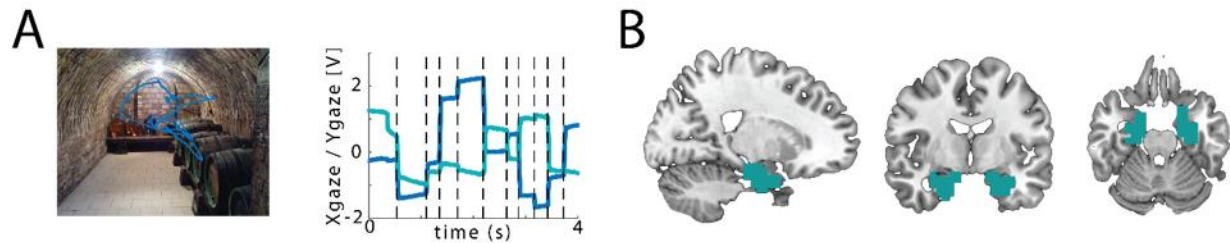
33 Grid cells are one of the core building blocks of spatial navigation [1]. Single cell recordings of grid cells in
34 the rodent entorhinal cortex revealed hexagonal coding of the local environment during spatial navigation
35 [1]. Grid-like activity has also been identified in human single cell recordings during virtual navigation [2].
36 Human fMRI studies further provide evidence that grid-like signals are also accessible on a macroscopic
37 level [3-7]. Studies in both non-human primates [8] and humans [9, 10] suggest that grid-like coding in the
38 entorhinal cortex generalizes beyond spatial navigation during locomotion, providing evidence for grid-
39 like mapping of visual space during visual exploration - akin to the grid cell positional code in rodents
40 during spatial navigation. However, electrophysiological correlates of the grid-code in humans remain
41 unknown. Here, we provide evidence for grid-like, hexadirectional coding of visual space by human high
42 frequency activity, based on two independent data sets: non-invasive magnetoencephalography (MEG) in
43 healthy subjects and entorhinal intracranial EEG recordings in an epileptic patient. Both data sets
44 consistently show a hexadirectional modulation of broadband high frequency activity (60-120 Hz). Our
45 findings provide first evidence for a grid-like MEG signal, indicating that the human entorhinal cortex
46 codes visual space in a grid-like manner [8-10] and support the view that grid-coding generalizes beyond
47 environmental mapping during locomotion [4-6, 11]. Due to its millisecond accuracy, MEG recordings
48 allow to link grid-like activity to epochs during relevant behavior, thereby opening up the possibility for
49 new MEG-based investigations of grid coding at high temporal resolution.

50

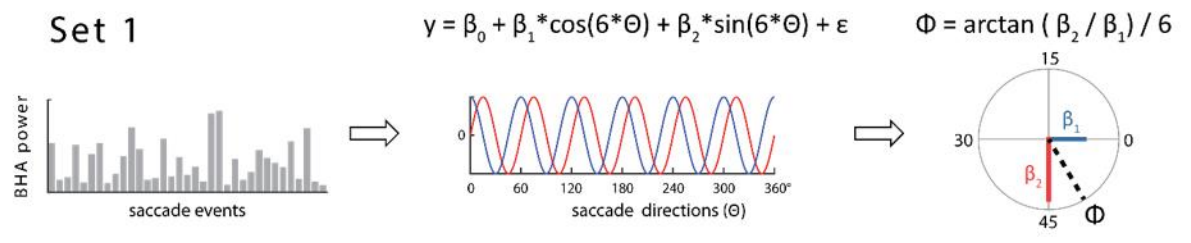
51

52 **Results**

53 The present study set out to investigate the electrophysiological basis of grid-like, hexadirectional coding
54 during visual exploration in humans, by simultaneously recording MEG and eye-tracking data from 35
55 healthy participants during free viewing of natural scenes (Fig. 1a), and simultaneously recording
56 intracranial EEG and eye-tracking data with depth electrodes in the entorhinal cortex of one epilepsy
57 patient (Fig. S1). Although the exact physiology of the broadband high frequency activity (BHA) remains
58 to be discovered, it has been shown to correlate with local neural activity [12-15]. Building on this and
59 other work demonstrating high frequency activity in the entorhinal cortex of behaving rodents [16], we
60 hypothesized to find a grid-like modulation of neuromagnetic BHA in the anterior medial temporal lobe
61 (MTL; Fig. 1b) and sought to verify the MEG findings in the intracranial recordings.

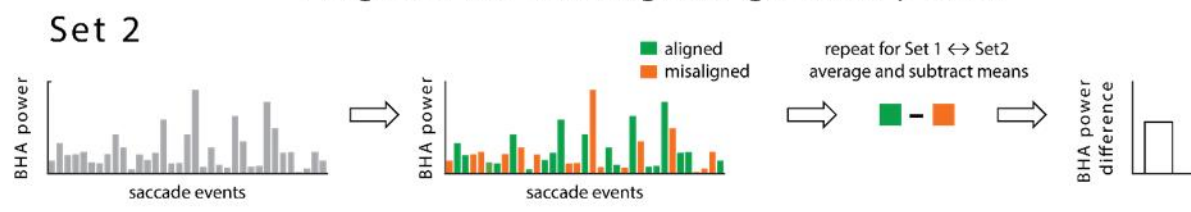


C Estimation of putative grid orientation



fit regressors for sine and cosine of saccade directions Θ with 60° periodicity to Set 1

Aligned vs. misaligned gamma power



aligned directions: $\Phi (\pm 15^\circ, \text{modulo } 60^\circ)$; misaligned directions: $\Phi + 30^\circ (\pm 15^\circ, \text{modulo } 60^\circ)$

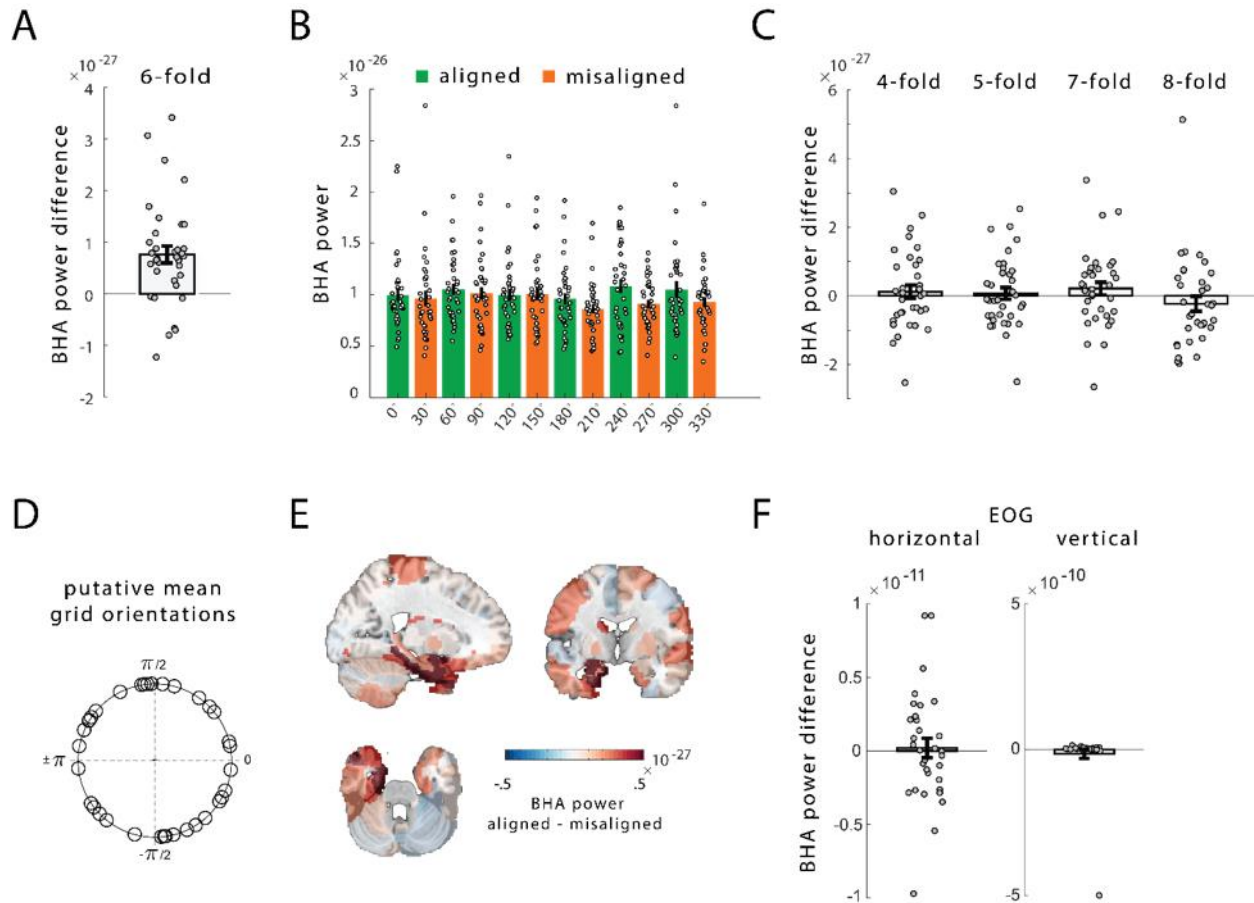
62
63 **Figure 1. Hexadirectional mapping of visual space: Procedure and Analysis.** (A) Paradigm: Free viewing
64 of 100 indoor and 100 outdoor scenes with simultaneous eye tracking (left). MEG data are aligned to
65 saccade onsets, defining events of interest (right). (B) Region-of-interest (highlighted), comprising
66 bilateral anterior portions of the hippocampus and parahippocampal gyrus. (C) Analysis rationale. Data
67 was split into halves (set 1, set 2) to estimate the putative grid orientation (angle of hexadirectional
68 activity) separately from computing aligned and misaligned BHA power, in a two-fold cross-validation
69 design. Estimation of putative grid orientation was done by fitting regressors for sine and cosine of
70 saccade directions (Θ) in the respective rotational symmetric space (here: 60° periodicity) to set 1 BHA
71 power (the general linear model included a constant and saccade duration as nuisance regressors).
72 Resulting beta estimates were used to derive the putative grid orientation angle (Φ). Trials in set 2 were
73 split according saccade directions aligned vs. misaligned to Φ . The difference in BHA power (aligned –
74 misaligned) reflects the grid-like modulation of BHA power.

75 **Grid-like modulation of source-localized broadband high frequency MEG data maps visual space**

76 MEG data were aligned to saccade onsets (Fig. 1a) and BHA power (60-120 Hz) source-localized to the
77 anterior MTL (Fig. 1b), was extracted during saccadic eye movements. We used a recently optimized MTL
78 source reconstruction method [17], extending prior MEG work localizing MTL activity [18-22]. Applying a
79 quadrature filter approach [3], we estimated the phase of hexadirectional activity as a function of saccade
80 direction (putative 'grid orientation') and subsequently quantified BHA power aligned and misaligned to
81 the main grid axis, in a two-fold cross-validation design (Fig. 1c). Estimation of the putative grid orientation
82 was achieved by fitting regressors for the sine and cosine of each saccade direction Φ in the respective
83 rotational symmetric space (e.g. 60°, 6-fold periodicity, along with biologically implausible 4-, 5-, 7- and 8-
84 fold control periodicities) to one half of the data (set 1) in a general linear model. Saccade length was
85 included as a nuisance regressor in the analysis. The resulting phase-angle was extracted from the
86 obtained beta coefficients ($\Phi = \arctan(\beta_1/\beta_2)/\text{symmetry}$), in the respective rotational symmetric space.
87 The other half of the data (set 2) was binned according to Θ , into aligned bins ($\Phi \pm 15^\circ$, modulo 60°) and
88 misaligned bins ($\Phi + 30^\circ \pm 15^\circ$, modulo 60°). This procedure was repeated after swapping set 1 and set
89 2, and power was averaged across the repetitions for aligned and misaligned bins, respectively.

90 We found significantly higher 60° periodic BHA (60-120 Hz) for aligned versus misaligned directional
91 sampling in the left anterior MTL, including entorhinal cortex ($t_{34} = 4.53$, $p < .00007$, Fig. 2a; Cohen's d
92 = .1988, reflecting a small effect size). When inspecting the 6 aligned and 6 misaligned 30° bins, aligned
93 directions generally elicited higher BHA power than misaligned directions (Fig. 2b), indicating that the
94 effect is not driven by a single direction. The putative grid orientations (i.e. the angle of the hexadirectional
95 modulation) did not cluster across participants (Fig. 2d). A 2x5 repeated-measures ANOVA with factors
96 alignment (aligned vs. misaligned) and rotational symmetry (4-, 5-, 6-, 7-, and 8-fold), revealed a significant
97 interaction ($F_{3,305, 112.3, \text{Greenhouse-Geisser}} = 3.49$, $p < .015$). Importantly, the significant quadratic contrast
98 (quadratic $F = 10.8$, $p < .0025$; linear and cubic contrasts not significant) indicated a u-inverted shape of
99 the differences across the rotational symmetries, being optimal for the 6-fold symmetry. Planned post-
100 hoc comparisons revealed that the difference for the 6-fold symmetry was bigger than for any of the other
101 symmetries (all t_{34} 's > 2.26 , all p 's $< .03$, 2-sided, uncorrected). Moreover, the differences for 4-, 5-, 7-,
102 and 8-fold symmetry were not significantly different from zero (all t_{34} 's < 1.2 & > -1.1 , all p 's $> .27$, 2-sided,
103 uncorrected, Fig. 2e). A repeated-measures ANOVA for the aligned bins in the MEG data showed no
104 significant difference ($F_{34,5} = 2.05$, $p = .075$). A repeated-measures ANOVA comparing the difference

105 (aligned – misaligned) across bins indicated that the effect was more pronounced for some directions
 106 ($F_{34,5} = 2.28$, $p = .049$). No 6-fold modulation of BHA power was observed in right anterior MTL ($t_{34} = -.4$,
 107 $p > .68$).



108
 109 **Figure 2. Grid-like modulation of BHA MEG activity during visual exploration.** (A) BHA power (60-120 Hz)
 110 aligned to the putative grid orientation is significantly higher than misaligned BHA power in the left
 111 anterior MTL. (B) 6-fold symmetric modulation of the BHA power, visualizing the effect in (A). The x-axis
 112 depicts the difference between saccade directions and the estimated putative grid orientations. (C) Other
 113 rotational symmetries (4-, 5-, 7- and 8-fold) do not show significant differences between aligned and
 114 misaligned BHA power (D) Putative grid orientations across participants did not show clustering. (E)
 115 Whole-brain analysis shows clustering of highest differences (aligned vs. misaligned, 60-120 Hz, 6-fold
 116 symmetry) in the left temporal lobe. (F) No significant difference between aligned vs. misaligned BHA
 117 power, in horizontal nor vertical electrooculogram (EOG) data (available in 32 participants). Dots show
 118 data from all participants; Error bars show S.E.M. See also Figures S1 and S2.

119 In addition, a whole-brain analysis of the 60° periodic modulation confirms the findings from the region
120 of interest (ROI)-based analysis and shows clustering of the highest differences between aligned and
121 misaligned BHA power in the left MTL (Fig. 2e), supporting the spatial specificity of the effect. To
122 investigate whether the hexadirectional modulation was limited to BHA, we computed the 60° periodic
123 modulation of power in a lower frequency band (20-50 Hz). There was no significant difference between
124 aligned versus misaligned directional sampling in the left anterior MTL ($t_{34} = 1.179$, $p = .247$). Furthermore,
125 in the present analyses, we investigated MEG activity during eye movements, which may be affected by
126 oculomotor-related artefacts. However, a 60° periodic BHA power modulation could not be found when
127 oculomotor activity recorded via EOG electrodes was analyzed ($t_{34} = 0.296$, $p > .769$; $t_{34} = -.9347$, $p > .357$;
128 for horizontal and vertical EOG signals, respectively; Fig. 2f). Moreover, there was no significant difference
129 in number of saccades aligned to the putative grid orientation versus number of saccades misaligned for
130 4-, 5-, 6-, 7- and 8-fold rotational symmetries (see Fig. S2).

131 In order to investigate the possible electrophysiological origin and spatial specificity of the MEG results,
132 we analyzed intracranial data recorded from the entorhinal cortex of an epilepsy patient (Fig. S1a), while
133 the patient was performing a free viewing task. The BHA power difference (aligned – misaligned) was
134 significantly higher compared to a surrogate distribution in the 6-fold rotational symmetry ($p < .011$, 1-
135 sided; Fig. S1b&c). Biologically implausible 4-, 5-, 7-, and 8-fold symmetries did not show a significant
136 modulation of BHA power (all p 's $> .36$, one-sided; Fig. S1d), neither did a spatially adjacent amygdala
137 electrode (Fig. S1e) show a 6-fold rotational symmetry of BHA ($p > .36$; Fig. S1f&g). The difference between
138 the hexadirectional modulation of BHA in entorhinal cortex and amygdala was significantly higher than
139 expected by chance ($p < .013$).

140

141 **Discussion**

142 The present results provide the first evidence for a grid-like signal in non-invasive electrophysiological
143 recordings in humans: electromagnetic activity, source-localized to the anterior MTL, revealed a
144 hexadirectional modulation of BHA power (60 -120 Hz). Confirming these findings, intracranial field
145 potentials recorded in the entorhinal cortex of a patient also showed a hexadirectional modulation of BHA
146 power in the same frequency band. The whole-brain MEG as well as control analyses in the intracranial
147 data point towards the spatial specificity of the effect within the anterior MTL (including entorhinal
148 cortex). The millisecond accuracy of these recordings allow to link activity to epochs during the relevant

149 behavior, thereby overcoming limitations of other non-invasive techniques, such as fMRI. We found a
150 grid-like pattern in BHA power, which has been suggested to correlate with local neural activity [12-15],
151 indicating that grid-coding is detectable with mass-electrophysiological recordings, opening up the
152 possibility for new non-invasive investigations of grid coding in cognitive neuroscience at high temporal
153 resolution. We show that the grid-like modulation of electromagnetic and intracranial electrophysiological
154 activity is related to the exploration of visual space. This is in line with work in non-human primates
155 identifying cells in the MTL that fire in relation to the animal's gaze position [8, 23-25], rather than coding
156 location during locomotion, as well as very recent fMRI work in humans showing hexadirectional
157 modulations of entorhinal BOLD activity related to the exploration of visual space [9, 10]. Given the
158 fundamental differences in sensory dominance between rodents and primates, it seems plausible that
159 primates code location during exploration by locomotion and eye movements.

160 In sum, our results support the view that grid-like coding in the anterior MTL goes beyond mapping the
161 environment during locomotion [8-10] and that the grid cell system could provide a general neural code
162 underlying core cognitive functions in humans [4-6, 11].

163

164 **Acknowledgments**

165 We thank all of the participants, in particular the patient, for taking part in the study, Elliot Smith for his
166 help with intracranial data collection and the medical staff at the Department of Neurological Surgery,
167 Columbia University, for their support. This project has received funding from the European Union's
168 Horizon 2020 research and innovation programme under grant agreement No 661373 (Marie-Curie grant
169 awarded to T.S.). CFD's research is supported by the Max Planck Society; the Kavli Foundation; the
170 European Research Council (ERC-CoG GEOCOG 724836), the Centre of Excellence scheme of the Research
171 Council of Norway – Centre for Neural Computation (223262/F50), The Egil and Pauline Braathen and Fred
172 Kavli Centre for Cortical Microcircuits, the National Infrastructure scheme of the Research Council of
173 Norway – NORBRAIN (197467/F50); and the Netherlands Organisation for Scientific Research (NWO-Vidi
174 452-12-009; NWO-Gravitation 024-001-006; NWO-MaGW 406-14-114; NWO-MaGW 406-15-291). J.J.
175 received funding from the US National Institutes of Health (R01-MH104606, S10 OD018211) and the
176 National Science Foundation (BCS-1724243). C.E.S. received funding from the JS McDonnell Foundation
177 and the US National Institutes of Health (P50-MH109429, EY024776). S.A.S. received funding from the

178 Dana Foundation and the US National Institutes of Health (MH 106700). O.J. received funding from the
179 James S. McDonnell Foundation (220020448), the Wellcome Trust (207550), and the Royal Society
180 Wolfson Research Merit Award.

181

182 **Author Contributions**

183 T.S., O.J., and C.F.D. designed the experiment. T.S., O.J., and C.F.D. wrote the paper. T.S. collected the
184 data. T.S. performed the analyses. M.L. and C.E.S. designed, conducted the iEEG part of the study and
185 assisted in writing of the manuscript. S.A.S. implanted electrodes. J.J. provided electrode imaging
186 information

187

188 **Declaration of Interests**

189 The authors declare no competing interests.

190

191 **References**

- 192 1. Hafting, T., Fyhn, M., Molden, S., Moser, M.-B., and Moser, E.I. (2005). Microstructure of a spatial map in
193 the entorhinal cortex. *Nature* 436, 801.
- 194 2. Jacobs, J., Weidemann, C.T., Miller, J.F., Solway, A., Burke, J.F., Wei, X.X., Suthana, N., Sperling, M.R.,
195 Sharan, A.D., Fried, I., et al. (2013). Direct recordings of grid-like neuronal activity in human spatial
196 navigation. *Nat Neurosci* 16, 1188-1190.
- 197 3. Doeller, C.F., Barry, C., and Burgess, N. (2010). Evidence for grid cells in a human memory network.
198 *Nature* 463, 657.
- 199 4. Bellmund, J., Deuker, L., and Doeller, C. (2016). Grid-cell representations in mental simulation. *Elife* 5.
- 200 5. Horner, A.J., Bisby, J.A., Zotow, E., Bush, D., and Burgess, N. (2016). Grid-like Processing of Imagined
201 Navigation. *Curr Biol* 26, 842-847.
- 202 6. Constantinescu, A.O., O'Reilly, J.X., and Behrens, T.E.J. (2016). Organizing conceptual knowledge in
203 humans with a gridlike code. *Science* 352, 1464-1468.
- 204 7. Kunz, L., Schroder, T.N., Lee, H., Montag, C., Lachmann, B., Sariyska, R., Reuter, M., Stirnberg, R.,
205 Stocker, T., Messing-Floeter, P.C., et al. (2015). Reduced grid-cell-like representations in adults at genetic
206 risk for Alzheimer's disease. *Science* 350, 430-433.
- 207 8. Killian, N.J., Jutras, M.J., and Buffalo, E.A. (2012). A map of visual space in the primate entorhinal cortex.
208 *Nature* 491, 761.
- 209 9. Nau, M., Navarro Schroder, T., Bellmund, J.L.S., and Doeller, C.F. (2018). Hexadirectional coding of
210 visual space in human entorhinal cortex. *Nat Neurosci*.
- 211 10. Julian, J.B., Keinath, A.T., Frazzetta, G., and Epstein, R.A. (2018). Human entorhinal cortex represents
212 visual space using a boundary-anchored grid. *Nat Neurosci*.
- 213 11. Wilming, N., Konig, P., Konig, S., and Buffalo, E.A. (2018). Entorhinal cortex receptive fields are
214 modulated by spatial attention, even without movement. *Elife* 7.

- 215 12. Ray, S., Crone, N.E., Niebur, E., Franaszczuk, P.J., and Hsiao, S.S. (2008). Neural correlates of high-
216 gamma oscillations (60–200 Hz) in macaque local field potentials and their potential implications in
217 electrocorticography. *Journal of Neuroscience* 28, 11526-11536.
- 218 13. Mukamel, R., Gelbard, H., Arieli, A., Hasson, U., Fried, I., and Malach, R. (2005). Coupling between
219 neuronal firing, field potentials, and fMRI in human auditory cortex. *Science* 309, 951-954.
- 220 14. Manning, J.R., Jacobs, J., Fried, I., and Kahana, M.J. (2009). Broadband shifts in local field potential
221 power spectra are correlated with single-neuron spiking in humans. *Journal of Neuroscience* 29, 13613-
222 13620.
- 223 15. Lachaux, J.-P., Axmacher, N., Mormann, F., Halgren, E., and Crone, N.E. (2012). High-frequency neural
224 activity and human cognition: past, present and possible future of intracranial EEG research. *Progress in*
225 *neurobiology* 98, 279-301.
- 226 16. Chrobak, J.J., and Buzsaki, G. (1998). Gamma oscillations in the entorhinal cortex of the freely behaving
227 rat. *J Neurosci* 18, 388-398.
- 228 17. Backus, A.R., Schoffelen, J.M., Szebenyi, S., Hanslmayr, S., and Doeller, C.F. (2016). Hippocampal-
229 Prefrontal Theta Oscillations Support Memory Integration. *Curr Biol* 26, 450-457.
- 230 18. Kaplan, R., Doeller, C.F., Barnes, G.R., Litvak, V., Düzel, E., Bandettini, P.A., and Burgess, N. (2012).
231 Movement-related theta rhythm in humans: coordinating self-directed hippocampal learning. *PLoS biology*
232 10, e1001267.
- 233 19. Fuentemilla, L., Barnes, G.R., Düzel, E., and Levine, B. (2014). Theta oscillations orchestrate medial
234 temporal lobe and neocortex in remembering autobiographical memories. *Neuroimage* 85 Pt 2, 730-737.
- 235 20. Staudigl, T., and Hanslmayr, S. (2013). Theta oscillations at encoding mediate the context-dependent
236 nature of human episodic memory. *Curr Biol* 23, 1101-1106.
- 237 21. Heusser, A.C., Poeppel, D., Ezzyat, Y., and Davachi, L. (2016). Episodic sequence memory is supported by
238 a theta-gamma phase code. *Nat Neurosci* 19, 1374-+.
- 239 22. Guitart-Masip, M., Barnes, G.R., Horner, A., Bauer, M., Dolan, R.J., and Düzel, E. (2013).
240 Synchronization of Medial Temporal Lobe and Prefrontal Rhythms in Human Decision Making. *The*
241 *Journal of Neuroscience* 33, 442-451.
- 242 23. Rolls, E.T., Robertson, R.G., and Georges-François, P. (1997). Spatial view cells in the primate
243 hippocampus. *European Journal of Neuroscience* 9, 1789-1794.
- 244 24. Wirth, S., Baraduc, P., Planté, A., Pinède, S., and Duhamel, J.-R. (2017). Gaze-informed, task-situated
245 representation of space in primate hippocampus during virtual navigation. *PLoS biology* 15, e2001045.
- 246 25. Meister, M.L., and Buffalo, E.A. (2018). Neurons in primate entorhinal cortex represent gaze position in
247 multiple spatial reference frames. *Journal of Neuroscience* 38, 2430-2441.
- 248 26. Berens, P. (2009). CircStat: A MATLAB Toolbox for Circular Statistics. *J Stat Softw* 31, 1-21.
- 249 27. Oostenveld, R., Fries, P., Maris, E., and Schoffelen, J.M. (2011). FieldTrip: Open source software for
250 advanced analysis of MEG, EEG, and invasive electrophysiological data. *Comput Intell Neurosci* 2011,
251 156869.
- 252 28. Penny, W.D., Friston, K.J., Ashburner, J.T., Kiebel, S.J., and Nichols, T.E. (2011). Statistical parametric
253 mapping: the analysis of functional brain images, (Elsevier).
- 254 29. Avants, B.B., Tustison, N., and Song, G. (2009). Advanced normalization tools (ANTs). *Insight j* 2, 1-35.
- 255 30. Staudigl, T., Hartl, E., Noachtar, S., Doeller, C.F., and Jensen, O. (2017). Saccades are phase-locked to
256 alpha oscillations in the occipital and medial temporal lobe during successful memory encoding. *PLoS Biol*
257 15, e2003404.
- 258 31. Stolk, A., Todorovic, A., Schoffelen, J.M., and Oostenveld, R. (2013). Online and offline tools for head
259 movement compensation in MEG. *Neuroimage* 68, 39-48.
- 260 32. Engbert, R., and Kliegl, R. (2003). Microsaccades uncover the orientation of covert attention. *Vision Res*
261 43, 1035-1045.
- 262 33. Tzourio-Mazoyer, N., Landeau, B., Papathanassiou, D., Crivello, F., Etard, O., Delcroix, N., Mazoyer, B.,
263 and Joliot, M. (2002). Automated anatomical labeling of activations in SPM using a macroscopic
264 anatomical parcellation of the MNI MRI single-subject brain. *Neuroimage* 15, 273-289.
- 265 34. Nolte, G. (2003). The magnetic lead field theorem in the quasi-static approximation and its use for
266 magnetoencephalography forward calculation in realistic volume conductors. *Phys Med Biol* 48, 3637-
267 3652.

- 268 35. Gross, J., Kujala, J., Hamalainen, M., Timmermann, L., Schnitzler, A., and Salmelin, R. (2001). Dynamic
269 imaging of coherent sources: Studying neural interactions in the human brain. *Proc Natl Acad Sci U S A*
270 *98*, 694-699.
- 271 36. Jacobs, J., Miller, J., Lee, S.A., Coffey, T., Watrous, A.J., Sperling, M.R., Sharan, A., Worrell, G., Berry,
272 B., Lega, B., et al. (2016). Direct Electrical Stimulation of the Human Entorhinal Region and Hippocampus
273 Impairs Memory. *Neuron* *92*, 983-990.
- 274 37. Maris, E., and Oostenveld, R. (2007). Nonparametric statistical testing of EEG- and MEG-data. *J Neurosci*
275 *Methods* *164*, 177-190.

276

277 **Star Methods**

278

279 **Contact for Reagent and Resource Sharing**

280 Further information and requests for resources and reagents should be directed to and will be fulfilled by
281 the Lead Contact, Tobias Staudigl (tobias.staudigl@cshs.org).

282 **Experimental Model and Subject Details**

283 36 young healthy adults were included in the MEG study. Initially, 48 participants were recruited;
284 however, 12 dropped out due to not completing the study (7 participants did not come back for one of
285 the sessions, see below), excessive movement artifacts (2 participants) and technical problems during the
286 recordings (3 participants). The 36 participants included in this study (24 females; mean age 23.1 years,
287 range 18-30 years; 35 right handed) reported no history of neurological and/or psychiatric disorders and
288 had normal or corrected-to-normal vision. One participant was excluded from the analysis due to
289 insufficient number of trials. Parts of this data have been published in Staudigl, et al. [30] with respect to
290 independent research questions and analyses. All participants gave written informed consent before the
291 start of experiment in accordance with the Declaration of Helsinki. The study was approved by the local
292 ethics committee (commission for human related research CMO-2014/288 region Arnhem/Nijmegen NL).
293 Additionally, one male patient (age range 25-45) with a history of drug resistant epilepsy was included in
294 the study. The patient, who volunteered to participate in the study at Columbia University Medical School,
295 had depth electrodes implanted for diagnostic reasons. All procedures were approved by the Institutional
296 Review Board at Columbia University Medical School. The patient provided informed consent before
297 participating in the study and was free to withdrawn from the study at any point. The study was approved
298 by the Institutional Review Board at Columbia University Medical School, New York City, US.

299

300 **Method Details**

301 **Design, Procedure and Materials.**

302 The design for the healthy participants comprised an MEG and an fMRI (not reported here) session. The
303 session order was counterbalanced across participants. Three stimulus sets, consisting of 100
304 photographs each, were constructed for each session. Half of the photographs were outdoor scenes, the
305 other half indoor scenes (see Fig. 1a, for an example). The photographs were presented on a 39 x 46 cm
306 back-projection screen in the MEG chamber, subtending a visual angle of approximately 27° × 32°. Two
307 stimulus sets were presented during encoding, all three sets during test. Assignment of set to encoding or

308 test was counterbalanced across participants. Nine additional scenes were presented during a short
309 practice session before encoding and test in order to explain the task. Participants were made aware
310 about the memory test before the start of the experiment. During the study phase, photographs were
311 presented for 4 s. The order was randomized with the constraint that no more than four scenes of the
312 same type (indoor / outdoor) were shown consecutively. The participants were instructed to judge the
313 scene type (indoor / outdoor) via a button press during the fixation cross (variable duration of 1 – 2 s)
314 following each scene (mean accuracy = .954, std = .068). This encoding task was chosen to ensure
315 attention to each scene. Participants were not expected to fixate, i.e. they freely viewed the scenes. The
316 study phase was followed by a distracter phase (solving simple mathematical problems for ~ 1 min), ~5
317 min of fixation to different locations on the screen used to evaluate eye tracker accuracy, and ~1 min of
318 eyes open and ~1 min of eyes closed. Subsequently, participants performed a recognition memory test
319 followed. Only data from the study phase are presented here.

320

321 **MEG Acquisition and Preprocessing.**

322 MEG was recorded in a magnetically shielded room, using a 275 whole-brain axial gradiometer system
323 (VSM MedTech/CTF MEG, Coquitlam, Canada). The data were sampled at a rate of 1200 Hz following a
324 low-pass anti-aliasing filter with a cutoff at 300 Hz. In addition, we recorded vertical and horizontal
325 electro-oculograms from bipolar Ag/AgCl electrodes (<10k Ω impedance; available for 32 participants)
326 placed below and above the left eye and at the bilateral outer canthi. 3 head coils placed at anatomical
327 landmarks (nasion and both ear canals) were used to track the position of the head relative to the MEG
328 helmet during the recordings. The head position was continuously monitored using a real-time head
329 localizer [31]. Each participant's nasion, left and right ear canal, and head shape were digitized with a
330 Polhemus 3Space Fasttrack. Data preprocessing was done using the Fieldtrip [27] toolbox. Data were
331 divided into single epochs, ranging from 0 to 4 s after scene onset, and corrected for cardiac artifacts using
332 Independent Component Analysis (ICA).

333

334 **Eye Tracking Acquisition, Analyses and Trial Definition.**

335 Eye tracking data were recorded simultaneously with MEG data. We tracked the horizontal and vertical
336 movements of each participant's left eye with an Eyelink 1000 (SR Research) eye tracker. The eye tracker
337 was calibrated before recording data, by collecting gaze fixation samples from known target points to map
338 raw eye data onto screen coordinates. Participants fixated nine dots sequentially appearing on a 3 by 3

339 grid. During the subsequent validation run, the difference between current gaze fixations and fixations
340 during the calibration were obtained. If this difference was smaller than 1 degree visual angle, the
341 calibration was accepted. Vertical and horizontal eye movements were transformed into velocities.
342 Velocities exceeding a given threshold (velocity > 6 x the standard deviation of the velocity distribution,
343 duration > 12 ms, see Engbert and Kliegl [32]) were defined as saccades. Saccade onsets during scene
344 presentation in the study phase defined the events of interest (trials). Only trials that were free of other
345 saccades and blinks in a 200 ms interval after saccade onset were included. On average, 558 (std = 196.9)
346 trials remained for the analysis. The trials were zero-padded to a length of 0.6 s (i.e., adding 200 ms of
347 zeros before and after the 200 ms of data). One participant was excluded from the analysis due to
348 insufficient number of trials for the hexadirectional analysis.

349 We focused our analysis on high frequency activity because it has been shown to correlate with local
350 neural activity [12-15] and was reported in the entorhinal cortex of behaving rodents [16]. We did not
351 analyze lower frequencies (e.g., theta) because our data epochs were too short to obtain a reasonable
352 frequency resolution in these bands.

353

354 **Source Reconstruction.**

355 Based on our a priori hypothesis on the origin of the grid signal in the entorhinal cortex, we performed a
356 region-of-interest based source reconstruction. To account for the spatial resolution of MEG, we
357 constructed two anterior medial temporal ROIs, comprising the anterior portions of the hippocampus and
358 parahippocampal gyrus in the left and right hemisphere, respectively (Figure 1b). For each hemisphere,
359 we aimed at computing one leadfield generated by the entire ROI, rather than averaging across multiple
360 point sources constructed within each ROI, applying a recently optimized MTL source reconstruction
361 method [17].

362 To construct the anterior medial temporal ROIs, we created 5 mm grids covering the voxels inside the
363 anterior half (median split) of anatomical masks including the labels 'Hippocampus_L',
364 'ParaHippocampal_L' and 'Hippocampus_R', 'ParaHippocampal_R', respectively, based on the Automatic
365 Anatomical Labeling atlas in Montreal Neurological Institute space [33].

366 For each participant, the MNI grid was warped onto each participant's anatomy bases on individual
367 structural MR images (1 mm isotropic voxels), acquired on a 3T Siemens Magnetom Prisma MRI system
368 (Siemens, Erlangen, Germany), after aligning the structural images to the MEG coordinate system, utilizing
369 the fiducials (nasion, left and right preauricular points) and individual head-shapes recorded after the

370 experiment. A realistic single-shell brain volume conduction model [34] was constructed for each
371 participant, based on these structural MRIs.

372 On the basis of this model, the contribution of dipolar sources at each grid point to the sensor level data
373 was estimated. Singular value decomposition was then used to reduce the columns of this sensor-by-grid
374 point leadfield matrix. The vector explaining most variance was selected, resulting in a leadfield matrix
375 consisting of one spatial component for each anterior medial temporal lobe ROI.

376 The cross-spectral density for the construction of the spatial filters was derived from the Fourier
377 transformation of all trials (epoch 0 to 200 ms from saccade onset) at the frequency of interest (90 Hz)
378 with 30 Hz spectral smoothing using a multitaper approach with 11 tapers from discrete prolate spheroidal
379 sequences (dpss). The cross-spectrum was regularized prior to matrix inversion by loading the diagonal of
380 the matrix with 5% of the average sensor power. We employed the Dynamic Imaging of Coherent Sources
381 (DICS) beamformer [35] to construct a spatial filter for each specified location. The sensor level single-trial
382 data was projected into source space by multiplying it with the spatial filter of each ROI, allowing for
383 further analysis to be conducted in virtual sensor space.

384 For the whole brain analysis (see Figure 2e), the same source estimation procedure was repeated for all
385 unique labels of the Automatic Anatomical Labeling atlas that include cortical brain areas.

386

387 **Hexadirectional analysis.**

388 The estimation of the hexadirectional signal followed a two-step procedure (see Fig. 1c): First, the putative
389 grid orientation was estimated on one half of the trials (a trial was defined by the onset of individual
390 saccades, see above). Second, aligned and misaligned (to the estimated putative grid orientation)
391 broadband high frequency activity (BHA) (60-120 Hz) power was computed. The procedure was repeated
392 with inversed assignment of data sets to the two steps, and aligned and misaligned BHA power was
393 averaged across the repetitions (two-fold cross-validation design).

394 Because of a horizontal bias in the distribution of saccade directions, we removed trials such that the
395 distribution of saccade directions in the analyses did not differ from a uniform distribution within
396 participants (Rayleigh-test, all p-values > .05). Performing a 4-,5-,6-,7- and 8-fold analyses of the saccades
397 directions yielded no significant difference between the number of saccades aligned and misaligned to
398 the putative grid orientation (4-fold: $t_{34} = -1.673$, $p=.104$; 5-fold: $t_{34} = -1.202$, $p=.238$; 6-fold: $t_{34} = -.392$,
399 $p=.698$; 7-fold: $t_{34} = -.82$, $p=.418$; 8-fold: $t_{34} = -.986$, $p=.3310$; see Fig. S2).

400 The remaining data was split into halves (set 1, set 2), and BHA power was computed for each set in virtual
401 sensor space by applying a sliding time window approach with a window length of 44 ms length in steps
402 of 10 ms across the data to each trial (epoched from saccade on- to offset, individual for each trial). After
403 multiplying a hanning taper to each window, the Fourier transformation was calculated at the frequency
404 of interest (90 Hz) with 30 Hz spectral smoothing using a multitaper approach with 2 dpss tapers. BHA
405 power was averaged across time bins within each trial, in cases where more than one BHA value resulted
406 from the sliding time window approach.

407 To estimate the putative grid orientation, regressors (β_1 , β_2) for sine and cosine of saccade directions (Θ)
408 in the respective rotational symmetric space (6-fold symmetry = 60° periodicity) were fitted to set 1 BHA
409 power using a general linear model including the saccade length (sl) as a nuisance regressor:

$$410 \quad y = \beta_0 + \beta_1 * \cos(6 * \theta) + \beta_2 * \sin(6 * \theta) + \beta_3 * sl + \varepsilon$$

411 Resulting beta estimates were used to derive the putative grid orientation (Φ):

$$412 \quad \Phi = \arctan(\beta_1 + \beta_2) / \text{symmetry}$$

413 The other half of the data (set 2) was binned according to each trial's saccade direction Θ , into aligned
414 bins ($\Phi \pm 15^\circ$, modulo 60°) and misaligned bins ($\Phi + 30^\circ \pm 15^\circ$, modulo 60°). BHA power was averaged
415 for aligned and misaligned bins, respectively.

416 After repeating the procedure with inversed assignment of data sets to the two steps, power was
417 averaged across the repetitions for aligned and misaligned bins, respectively. The difference in BHA power
418 (aligned – misaligned) reflects the grid-like modulation of BHA power. Biologically implausible 4-, 5, 7- and
419 8-fold periodicities were computed with the same approach and compared to the 6-fold periodic
420 modulation of BHA power.

421

422 **Intracranial data.**

423 One male patient (age range 25-45) with a history of drug resistant epilepsy was included in the study.
424 The patient was implanted with intracranial EEG electrodes for diagnostic purposes. Recordings were
425 performed at the Department of Neurological Surgery, Columbia University, USA. All procedures were
426 approved by the Institutional Review Board at Columbia University Medical School. The patient provided
427 informed consent before participating in the study and was free to withdrawn from the study at any point.

428 The procedure and design of the study was similar to the MEG procedure and design. The patient
429 performed a free viewing task with 80 coloured images (indoor and outdoor scene, faces, animals, etc.)
430 as stimuli. Each image was presented for 6 s in the center of a screen at a distance of about 65 cm,
431 subtending a visual angle of approx. $18^\circ \times 12^\circ$. The patient was requested to freely view each image. After
432 the stimulus offset a gray screen was displayed with five possible response options. The participant was
433 asked to indicate how he liked the last image on a scale ranging from 1 (very little) to 5 (very much) via
434 button press. The next image was displayed with a jitter interval of 0.1 to 0.5 s.

435 The locations of the electrodes were determined using pre- and post-operative MRIs and CTs, respectively
436 (for details see Jacobs, et al. [36]). One contact was identified to be fully located within the left entorhinal
437 cortex (indicated by red crosshair in Fig. S1A) and field potentials from this contact were used for further
438 analysis. To investigate spatial specificity of the hexadirectional modulation, a contact in the amygdala,
439 neighboring the entorhinal cortex (see Fig. S1E), was used to as a control site.

440 Intracranial EEG was recorded from depth electrodes (PMT Corporation) with multiple recording sites
441 (inter-contact spacing = 5 mm), using a Blackrock system (Blackrock Microsystems, Inc., Salt Lake City,
442 USA), with voltages referenced to an intracranial electrode site with least signal (2000 Hz sampling rate).
443 Data was re-referenced offline using a bipolar montage. Entorhinal data was re-referenced to the
444 contact's medial neighbor. Amygdala data was re-referenced to its lateral neighbor. A bipolar montage
445 provides high spatial specificity with respect to the underlying electric source and low susceptibility to
446 volume conducted artifacts (e.g. oculomotor artifacts).

447 Eye movements were monitored with a Tobii TX300 eye tracker. The left and right eye positions were
448 sampled at 300Hz. A five-point calibration was performed prior to experimental session. Intracranial EEG
449 data was offline downsampled to 1000 Hz and eye tracking data was interpolated to match sampling rate
450 at 1kHz. Subsequently, eye tracking and intracranial EEG data were co-registered and segmented into
451 epochs with 0.1 sec of prestimulus interval and 6 sec of stimulus presentation. All epochs were visually
452 inspected for artifacts (e.g. epileptiform spikes). Contaminated epochs were excluded from the analyses.

453 The eye tracking data was low-pass filtered at 30 Hz using a zero-phase forward and reverse butterworth
454 infinite impulse response filter.

455 Vertical and horizontal eye movements of the left eye were transformed into velocities. Velocities
456 exceeding a given threshold (velocity > 6 x the standard deviation of the velocity distribution, duration >
457 12 ms, see Engbert and Kliegl [32]) were defined as saccades. Saccade onsets during scene presentation

458 in the study phase defined the events of interest (trials). Only trials that were free of other saccades and
459 blinks in a 200 ms interval after saccade onset were included.

460 Intracranial EEG data were aligned to saccade onsets and BHA power was extracted during saccadic eye
461 movements. The trials were zero-padded to a length of 0.6 s (i.e., adding 200 ms of zeros before and after
462 the 200 ms of data). The estimation of the hexadirectional signal was identical to the procedure described
463 above (see Hexadirectional Analysis).

464

465 **QUANTIFICATION AND STATISTICAL ANALYSIS**

466 We tested the null-hypothesis that there is no difference between BHA power for aligned versus
467 misaligned saccade directions, in the left and right ROIs for the 6-fold rotational symmetry, using 2-sided
468 t-tests. To control for multiple comparisons, we adopted a significance level of 0.025. To measure effect
469 size Cohen's d was computed as

$$470 \quad d = \frac{\bar{x}_1 - \bar{x}_2}{\sqrt{s_1^2 + s_2^2 - 2rs_1s_2}/\sqrt{2(1-r)}}$$

471 with r denoting Pearson's correlation coefficient.

472 A 2x5 repeated-measures ANOVA with factors alignment (aligned vs. misaligned) and rotational symmetry
473 (4-, 5-, 6-, 7-, and 8-fold) was used to investigate the effect in the left anterior MTL. Planned post-hoc
474 comparisons (2-sided t-tests, uncorrected) were used to test the difference for the 6-fold symmetry versus
475 the other symmetries (4-, 5-, 7-, and 8-fold) and to test whether BHA power in the left anterior MTL were
476 different from zero for the biologically implausible 4-, 5-, 7-, and 8-fold rotational symmetries.

477 A further repeated-measures 1-way ANOVA with the factor rotational symmetry (4-, 5-, 6-, 7-, and 8-fold)
478 was used to test for differences among aligned bins in the MEG BHA. To investigate whether the
479 hexadirectional modulation was limited to BHA, a post-hoc t-test (2-sided, alpha level = .05) was
480 performed to test the 60° periodic modulation of power in a lower frequency band (20-50 Hz). As a further
481 post-hoc control analysis, two t-test (2-sided, alpha = .05, uncorrected) were used to test a 60° periodic
482 BHA power modulation recorded on EOG electrodes (for horizontal and vertical EOG signals, respectively).
483 Five post-hoc t-tests (2-sided, alpha = .05, uncorrected) were used to test the difference in number of
484 saccades aligned to the putative grid orientation versus number of saccades misaligned to the putative

485 grid orientation (for 4-, 5-, 6-, 7- and 8-fold rotational symmetries, respectively). All of the above analyses
486 were performed on the group level with N = 35.

487 We did not include a whole brain statistical approach (as for example implemented in the MEG/EEG
488 Fieldtrip Toolbox), because a significant outcome in this kind of test would only speak to the null
489 hypothesis (no difference between conditions) being rejected and not provide information on the exact
490 spatial extent of the effect [37].

491 The intracranial BHA power differences (aligned – misaligned) in one patient were statistically quantified
492 by comparing them to a distribution of surrogate BHA power differences. The surrogate distribution of
493 BHA power differences was constructed by randomly assigning trials to the aligned and misaligned
494 condition, respectively. 50000 surrogate BHA power differences were computed. Intracranial BHA power
495 differences were compared to the 50000 surrogate BHA power differences, and considered to be
496 significant if they were larger than the 95 % of the surrogate BHA power differences (one-sided test). This
497 procedure was used to quantify the 6-fold periodic modulation of BHA power, as well as the biologically
498 implausible 4-, 5-, 7- and 8-fold periodicities. Additionally, the difference between the hexadirectional
499 modulation of BHA in entorhinal cortex (aligned – misaligned) and amygdala (aligned – misaligned) was
500 compared to a distribution of 50000 surrogate BHA power differences. Differences were considered to be
501 significant if they were larger than the 95 % of the surrogate BHA power differences (one-sided test).

502

503

504 **Data and Software Availability**

505 Data and custom-built MATLAB scripts are available from the authors upon request.

506

507

508

509

510 Current Biology, Volume 28

511

512 Supplemental Information

513

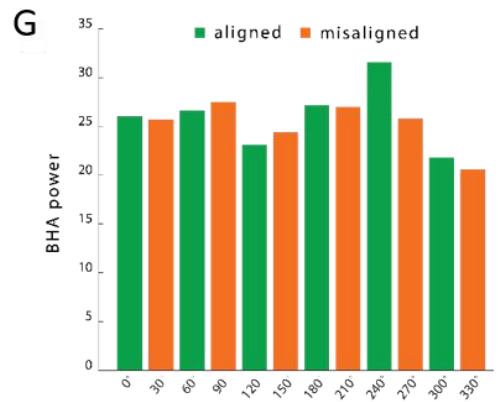
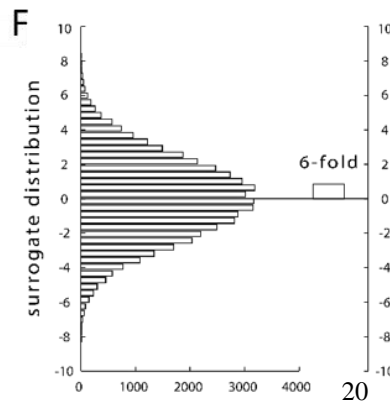
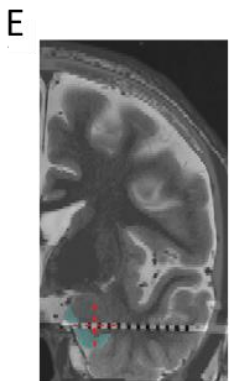
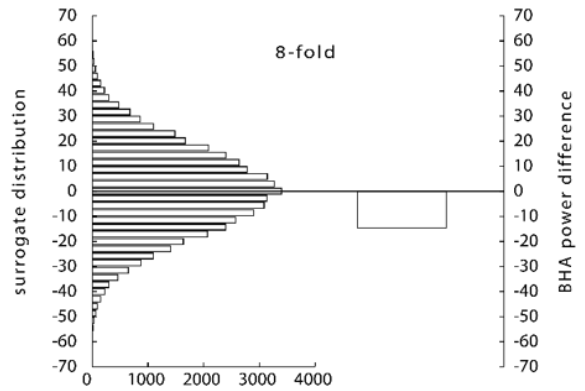
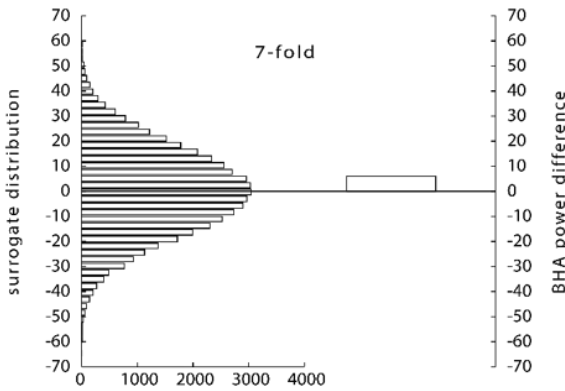
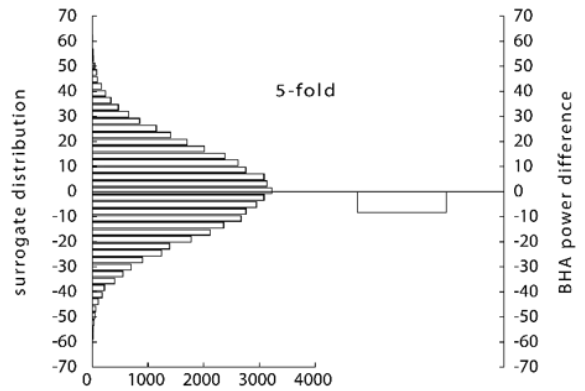
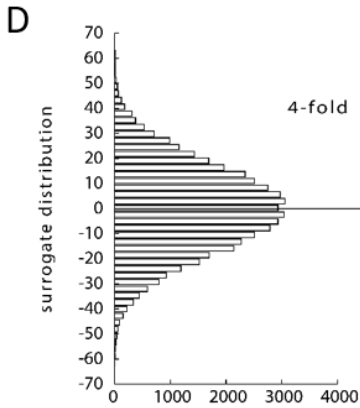
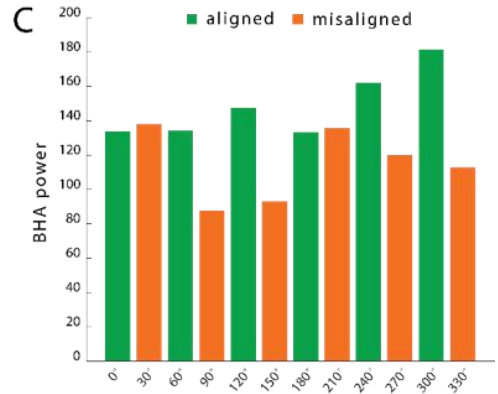
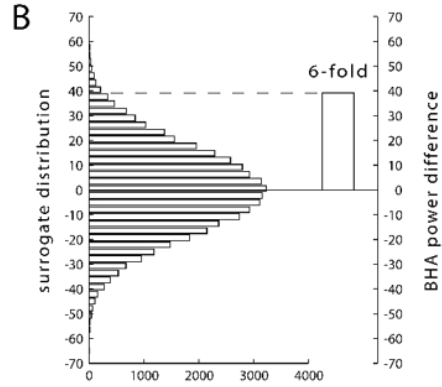
514 Hexadirectional Modulation of High-Frequency
515 Electrophysiological Activity in the Human
516 Anterior Medial Temporal Lobe Maps Visual Space

517

518 Tobias Staudigl, Marcin Leszczynski, Joshua Jacobs, Sameer A. Sheth, Charles E.
519 Schroeder, Ole Jensen, and Christian F. Doeller

520

521



523 **Figure S1. Intracranial data. Related to Figure 2.**

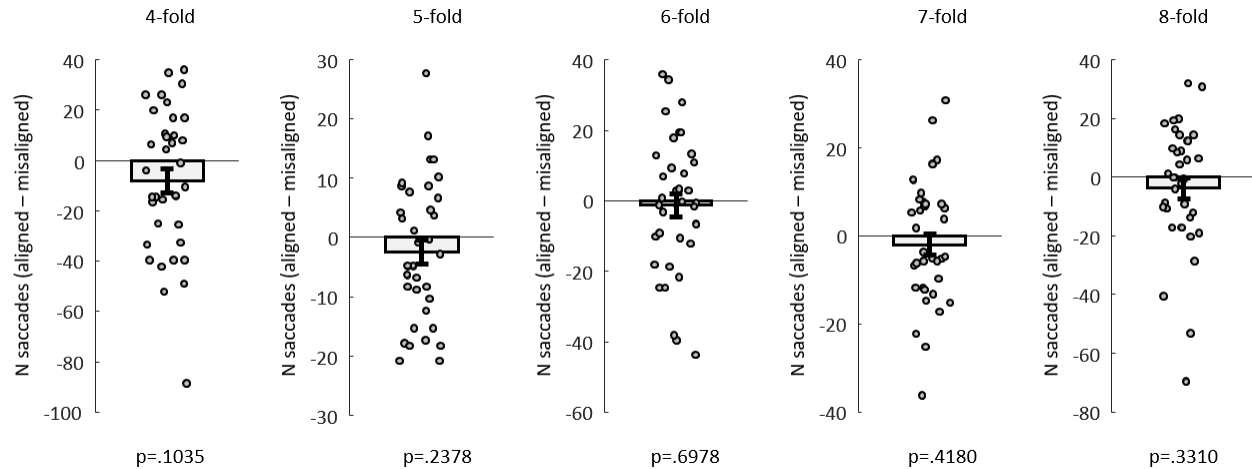
524 (A-C) Hexadirectional signal in intracranial entorhinal data. To investigate the possible electrophysiological
525 origin and spatial specificity of the MEG results, we analyzed intracranial data recorded from the
526 entorhinal cortex of an epilepsy patient, while the patient was performing a free viewing task. As for the
527 MEG data, intracranial data were aligned to saccade onsets and re-referenced using a bipolar montage to
528 provide high spatial specificity with respect to the underlying electric source. BHA power (60-120 Hz) was
529 extracted during saccadic eye movements and the hexadirectional analysis approach was applied (see
530 Figure 1c) (A) Electrode position. The red crosshair indicates the electrode position in the left entorhinal
531 cortex (highlighted). (B) BHA power difference (aligned vs. misaligned, 60-120 Hz, 6-fold symmetry, bar
532 plot) in the entorhinal electrode is significantly higher ($p < .011$) than the distribution of surrogate BHA
533 power differences, replicating the MEG findings. (C) 6-fold symmetric modulation of the BHA power,
534 visualizing the effect in (B), indicated that the effect is not driven by a single direction.

535 (D) Control periodicities in intracranial entorhinal data. Biological implausible rotational symmetries do
536 not show higher BHA power (60-120 Hz) for aligned versus misaligned saccade directions (4-fold: p
537 = .7135; 5-fold: p = .5753; 7-fold: p = .9573; 8-fold: p = .9868; one-sided tests). Bars represent BHA
538 difference, (aligned vs. misaligned), histograms the respective distribution of surrogate BHA power
539 differences.

540 (E-G) Intracranial control analyses. (E) Electrode position. The red crosshair indicates the electrode
541 position in the left amygdala, adjacent to but clearly outside the entorhinal cortex (highlighted). (F) BHA
542 power difference (aligned vs. misaligned, 60-120 Hz, 6-fold symmetry, bar plot) in the amygdala
543 electrode (bipolar montage) is not significantly higher ($p > .36$) than the distribution of surrogate BHA
544 power differences, confirming the spatial specificity of the hexadirectional modulation of BHA found in
545 the entorhinal cortex. (G) 6-fold symmetric modulation of the BHA power, visualizing the effect in (F).
546 The difference between the hexadirectional modulation of BHA in entorhinal cortex and amygdala was
547 significantly higher than expected by chance ($p < .013$) when compared to a distribution of surrogate
548 BHA power differences.

549

550



551
 552 **Figure S2. Hexadirectional modulation of saccade directions. Related to Figure 2.** There was no
 553 significant difference in number of saccades aligned to the putative grid orientation versus number of
 554 saccades misaligned for 4-, 5-, 6-, 7- and 8-fold rotational symmetries (all t 's > -1.6 and < 0 , all p 's $> .1$).
 555 The estimation of the hexadirectional modulation of the saccade direction followed a two-step procedure
 556 (see Figure 1c): First, the putative grid orientation was estimated on one half of the trials. BHA MEG
 557 activity during visual exploration in the left anterior temporal lobe was used during this step (analogous
 558 to the main analysis). Second, the number of saccades aligned and misaligned to the putative grid
 559 orientation were summed. The procedure was repeated with inversed assignment of data sets to the two
 560 steps, and the number of aligned and misaligned saccade directions was averaged across the repetitions
 561 (two-fold cross-validation design).

562

563